JGR | Machine Learning and Computation

RESEARCH ARTICLE
10.1029/2024JH000123

Forecasting 24-Hr Total Electron Content With Long Short-Term Memory Neural Network

Marjolijn Adolfs[1,2], Mohammed Mainul Hoque[1], and Yuri Y. Shprits[2,3,4]

[1]German Aerospace Center (DLR), Institute of Solar-Terrestrial Physics, Neustrelitz, Germany, [2]Institute of Physics and Astronomy, University of Potsdam, Potsdam, Germany, [3]Space Physics and Space Weather, Geophysics, GFZ German Research Centre for Geosciences, Potsdam, Germany, [4]Department of Earth, Planetary and Space Sciences, University of California Los Angeles, Los Angeles, CA, USA

Abstract An accurate prediction of the ionospheric state is important for correcting ionospheric propagation effects on Global Navigation Satellite Systems (GNSS) signals used in precise navigation and positioning applications. The main objective of the present work is to find a total electron content (TEC) model which gives a good estimate of ionospheric state not only during quiet but also during perturbed ionospheric conditions. For this, we implemented several long short-term memory (LSTM)-based models capable of predicting TEC up to 24 hr ahead. For the first time, we used the solar wind forcing parameters W_{prot} (a measure of the ionospheric disturbance during storm time) and E_{conv} (measure of the solar wind parameters) as driver parameters. We found that using external drivers does not improve the accuracy of TEC predictions significantly. The final model is trained with data from the last two solar cycles using TEC from the rapid UQRG global ionosphere maps (GIMs). Data from the years 2015 and 2020 were excluded from the training data set and used for testing. The performance of the LSTM-based TEC model is tested for near real-time (RT) cases as well by using RT products (IRTG GIMs) as historical TEC inputs. We compared the performance of the LSTM-based model to a quiet-time feed forward neural network (FNN)-based model and the Neustrelitz TEC model (NTCM). The results indicate that the LSTM-based model proposed here is outperforming the FNN-based model and NTCM in both cases, that is, using the UQRG or the IRTG GIMs as input for the historical TEC.

Plain Language Summary Knowledge of the ionospheric state is important for correcting ionospheric propagation effects on Global Navigation Satellite Systems (GNSS) signals used in precise navigation and positioning applications. The ionospheric state can be described by the total electron content (TEC). Here we propose a model that uses only the 3-day historical TEC, day of year, universal time, geographic longitude and latitude as input parameters and no other external drivers. The performance of the model has been analyzed for quiet and perturbed ionospheric conditions. The performance of the model is also tested for near real-time (RT) cases using the RT products from the International GNSS Service as an input for the historical TEC.

Key Points:

- We propose an LSTM-based model which can predict global TEC up to 24 hr ahead using the previous 3-day TEC history as input parameter
- The model is trained with data from two solar cycles (1998–2020) and the accuracy is analyzed for quiet and perturbed ionospheric conditions
- The near real-time (RT) performance of the model is also tested using the RT products from IGS as an input for the historical TEC

Correspondence to:
M. Adolfs,
Marjolijn.Adolfs@dlr.de

Citation:
Adolfs, M., Hoque, M. M., & Shprits, Y. Y. (2024). Forecasting 24-hr total electron content with long short-term memory neural network. *Journal of Geophysical Research: Machine Learning and Computation*, *1*, e2024JH000123. https://doi.org/10.1029/2024JH000123

Received 2 JAN 2024
Accepted 15 APR 2024

Author Contributions:
Conceptualization: Marjolijn Adolfs, Mohammed Mainul Hoque
Formal analysis: Marjolijn Adolfs, Mohammed Mainul Hoque
Funding acquisition: Mohammed Mainul Hoque
Methodology: Marjolijn Adolfs, Mohammed Mainul Hoque
Software: Marjolijn Adolfs
Supervision: Mohammed Mainul Hoque, Yuri Y. Shprits
Visualization: Marjolijn Adolfs
Writing – original draft: Marjolijn Adolfs
Writing – review & editing: Marjolijn Adolfs, Mohammed Mainul Hoque, Yuri Y. Shprits

1. Introduction

The ionosphere is an atmospheric layer which contains ionized particles, where ionization is mainly caused by solar radiation (Davies, 1990, p. 33). The state of the ionosphere is constantly varying due to space weather conditions. The ionosphere reacts to solar activity and geomagnetic storms (Lilensten, 2007, p. 125) and it's activity can be described by the total electron content (TEC) (Cherrier et al., 2017). The TEC is the line-of-sight number of free electrons and is given in TEC units (TECU), where one TECU stands for 10^{16} free electrons per square meter. Radio signals broadcasted by the Global Navigation Satellite System (GNSS) propagating through the ionosphere are affected by the free electrons, resulting in a delay (or advance) in the signal. One way to correct for this ionospheric effect is to use its dispersive property and combine multiple frequencies but this technique cannot be applied for single frequency users; instead, ionospheric models can be used. Single frequency receivers are still most commonly used in the mass market, aviation and automotive industry may be due to lower costs, power consumption and complexity. Therefore, it is important to utilize models that can correct for this propagation delay. Ionospheric models like Klobuchar (Klobuchar, 1987), NeQuick (Nava et al., 2008) or the Neustrelitz TEC model (NTCM) (Hoque et al., 2017, 2018, 2019; Hoque & Jakowski, 2015; Jakowski et al., 2011) can be used in order to predict the TEC. There are different kind of TEC models available, for example, broadcast or empirical models (listed above), physics-based- (e.g., Thermosphere-Ionosphere-Electrodynamics General

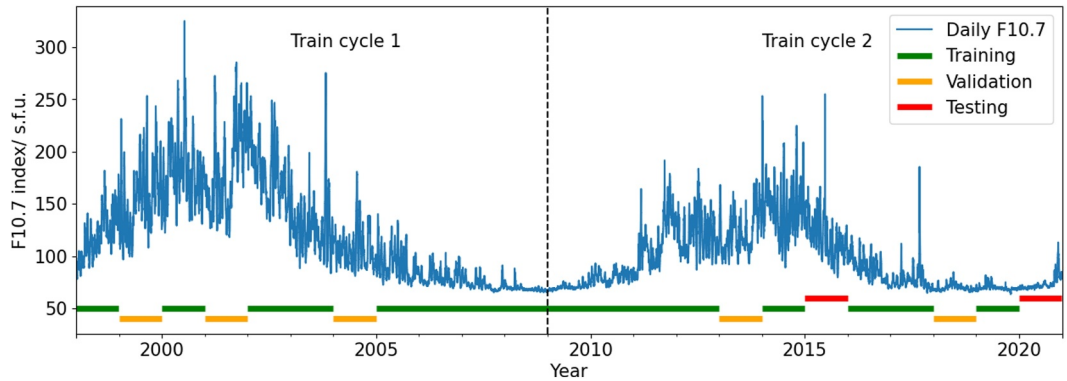

Figure 1. The solar flux index $F10.7$ plotted together with the training, validation and testing data set.

Circulation Model-TIE-GCM, Coupled Thermosphere Ionosphere Plasmasphere Electrodynamics Model-CTIPe) or neural network (NN)-based models. A lot of studies (Adolfs & Hoque, 2021; Chen et al., 2022; Cherrier et al., 2017; Chimsuwan et al., 2021; Li et al., 2023; Lin et al., 2022; Natras et al., 2022; Orus Perez, 2019; Sun et al., 2017; Tang et al., 2022; Xiong et al., 2021; Zewdie et al., 2021) have been applying different machine learning techniques for ionospheric TEC predictions. A few examples of the investigated architectures are feed forward neural networks (FNN) (Adolfs & Hoque, 2021; Orus Perez, 2019), long short-term memory (LSTM) (Chen et al., 2022; Chimsuwan et al., 2021; Sun et al., 2017; Zewdie et al., 2021) or different combinations, for example, convolutional neural network (CNN)-LSTM (Cherrier et al., 2017), CNN-LSTM-attention mechanism (Tang et al., 2022), encoder-decoder (ED)-LSTM extended (Xiong et al., 2021), ED-Convolutional LSTM (Li et al., 2023), decision trees and ensemble learning of tree-based learning algorithms (Natras et al., 2022). Not only the architectures are different for the individual models but also the prediction horizon, which can range from a few hours ahead up to multiple days, the region and the number of parameters that drive the models. The period covered by the studies is also varying. The NN-based model proposed here should make global predictions up to 24 hr ahead. Since geomagnetic storms can cause hugely disturbed TEC values, it is very important that the performance of ionospheric models is stable during these perturbed periods. A moderate storm event can be identified when the disturbance index *Dst* dropped below −50 nano tesla (nT) (Gonzalez et al., 1994). Our previous investigations in Adolfs et al. (2022) showed that the proposed storm-time model had a different performance for the individual storms. This indicates that the storms can be very different from each other. During the investigations only moderate and stronger storms were considered ($Dst < -50$ nT). Storms can be driven by coronal mass ejections (CMEs) or by high-speed solar-wind streams (HSS) which cause corotating interaction regions (CIRs). CMEs have a higher occurrence rate during the solar maximum with an irregular occurrence pattern, associated stronger *Dst* and sometimes a period of unusually calm geomagnetic activity before the storm whereas CIR driven storms have a higher occurrence rate during the declining phase of the solar cycle, a 27-day repeating occurrence pattern, weaker *Dst* and more frequently a calm before the storm (Borovsky & Denton, 2006). Our previous work (Adolfs et al., 2022; Adolfs & Hoque, 2021) was focussed on the FNN but this work focusses on using a different architecture, namely the LSTM. The LSTM architecture is known for its ability to perform well in time series forecasting because of its effective handling of long time lag tasks and can remember information for a long period of time. Therefore, this capability is exploited in TEC forecasting and the advantage of using this architecture over a traditional FNN architecture is investigated. Some of the models mentioned above, use geomagnetic indices and solar wind parameters to drive their models. Therefore, the advantage of including them is also investigated in this paper. The model is trained with global ionosphere maps (GIMs) from the Universitat Politècnica de Catalunya (UPC) international GNSS service (IGS) analysis center, that is, the UPC Quarter-of-an-hour time resolution Rapid GIMs (UQRG). The solar wind parameters are obtained from the OMNIWeb interface. Since the behavior of TEC during storms can be very different, it is important that data from the previous two solar cycles are included, so that the network can see more storms. The model's near real-time performance is investigated as well. Investigations about the delay in ionospheric response to solar parameters are out of scope but can be performed in the future. Even though the LSTM architecture is known for its effective handling of longer time lags, an improvement in performance may be achieved when this more accounted for.

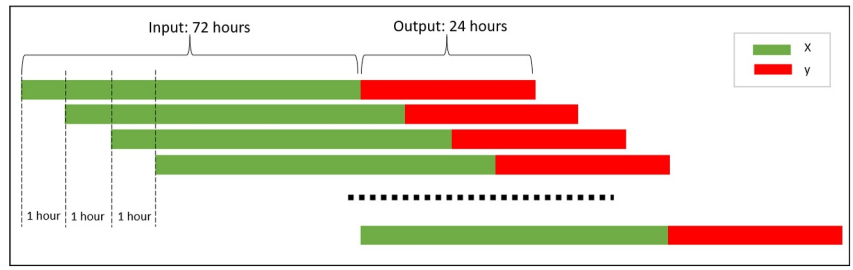

Figure 2. Sliding window technique using 72 hr of historic input data.

The paper is divided into different sections, where the first section includes a literature study about previous neural networks and a brief introduction to our proposed model as described above. Section 2 explains how the data is used to generate a database for training the neural network. The Methods section provides information about the LSTM architecture, hyperparameter tuning and feature selection. In Section 4, the results of the proposed model are analyzed and compared to existing models. The results are also shown for near real-time applications. In the last section we provide a short summary and conclusion (Section 5).

2. Data

The LSTM model is trained with TEC data from rapid UQRG GIMs using data from the previous two solar cycles (1998–2020), shown in Figure 1. The division into training, validation and testing data sets is shown in this figure as well, more information about the data division is given in Section 3 below.

The UQRG GIMs have been downloaded from ftp://newg1.upc.es/upc_ionex/ (accessed on 8 May 2022). Newer data (from the year 2022) was downloaded from the Crustal Dynamics Data Information System (CDDIS), available at https://cddis.nasa.gov/archive/gnss/ionex/ (accessed 10 March 2023). Since the correctness of the input data was out of scope in these investigations it may be beneficial to have a closer look at the accuracy of GIMs and perhaps including other techniques proposed in Chen et al. (2023) in the future. The rapid UQRG GIMs contain global TEC maps with a $5° \times 2.5°$ resolution of longitude and latitude, respectively. The TEC maps have a 15-min temporal resolution. To reduce the amount of data, the time resolution has been linearly interpolated to an hourly time resolution. Using hourly data reduces the computational complexity and therefore speeds up preprocessing and the training process. The geomagnetic storm indices such as *Hp*30 and *SYM-H* are downloaded from https://www.gfz-potsdam.de/en/hpo-index/ (accessed on 11 March 2023) and http://wdc.kugi.kyoto-u.ac.jp/aeasy/index.html (accessed on 10 March 2023), respectively. Again, we interpolated to an hourly time resolution for *Hp*30 and *SYM-H*. The solar flux index *F*10.7, the interplanetary magnetic field components *Bx*, *By*, and *Bz*, the solar wind bulk flow speed v_{sw}, the bulk flow latitude and longitude Lat_{sw}, Lon_{sw} and the proton density ρ_{prot}, with a time resolution of 1 hr, were downloaded from the OMNIWeb interface, available at https://omniweb.gsfc.nasa.gov/form/dx1.html (accessed 28 July 2023). The use of indices such as *Hp*30, *SYM-H* or *F*10.7 is common

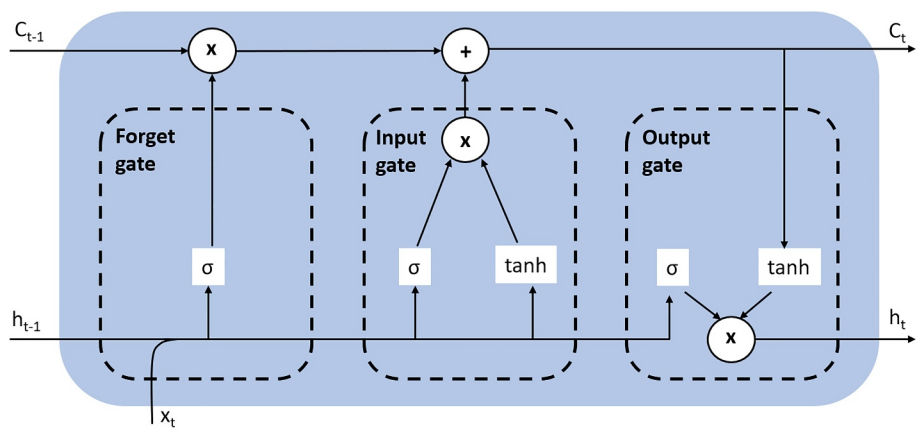

Figure 3. The general architecture of a long short-term memory (LSTM) cell together with the forget, input and output gate.

Table 1
The Hyperparameters and the Range of Search Investigated During Hyperparameter Tuning

Hyperparameter	Range of search
Learning rate	0.001, **0.0001**
Batch size	128, **256**, 512
Activation function	ReLU, **tanh**
Epochs	50, **100**
Architectures	20, **50**, 70, 100, 20–20, 50–20

Note. The selected hyperparameters are shown in bold.

but in this study the use of other parameters such as the E_{conv} and W_{prot} is investigated as well. The proton energy (W_{prot}) describes how deep the solar wind particles can penetrate in the atmosphere, causing ionization at lower layers. During storms, W_{prot} would become larger meaning the particles can penetrate deeper in the atmosphere and ionization levels are higher at lower layers. The *Dst* however, will show stronger negative *Dst* values due to the depression of the horizontal component of the magnetic field. Therefore, we use the W_{prot} as a substitute for *Dst* in order to use the solar wind parameters directly. The magnitude of the convection electric field (E_{conv}) can be used as a direct measure of the solar wind parameters, describing the coupling between the solar wind and the magnetosphere. The parameters can be defined by Kamal et al. (2020), for example,:

$$E_{conv} = |\vec{E}_{conv}| = |-\vec{v}_{sw} \times \vec{B}_{sw}| \tag{1}$$

$$\vec{v}_{sw} = v_{sw} \cdot \begin{Bmatrix} -\cos(Lat_{sw}) \cdot \cos(Lon_{sw}) \\ \cos(Lat_{sw}) \cdot \sin(Lon_{sw}) \\ \sin(Lat_{sw}) \end{Bmatrix} \tag{2}$$

$$W_{prot} = \frac{1}{2} \cdot \rho_{prot} \cdot v_{sw}^2 \tag{3}$$

where v_{sw} denotes the solar wind bulk flow speed, B_{sw} the interplanetary magnetic field vector, Lat_{sw} the bulk flow latitude, Lon_{sw} the bulk flow longitude and ρ_{prot} the proton density.

The sliding window technique has been chosen in order to make a supervised data set and the method is schematically shown in Figure 2. A time window of 24 hr of historic data was tested and following the authors in Cherrier et al. (2017), data with a time window of 72 hr was included in the investigations as well. Since the supervised data set becomes very large, it was randomly sampled by taking 60% of the data in case of 24 hr of historic input and in case of 72 hr by using 10%. During the testing phase, the model got tested with all the samples (data during 2015 and 2020) in order to make fair comparisons. The input shape for an LSTM network is number of samples, timesteps, features. The data has been reshaped to the needed input shape and saved as 3-dimensional Python NumPy arrays in a binary file.

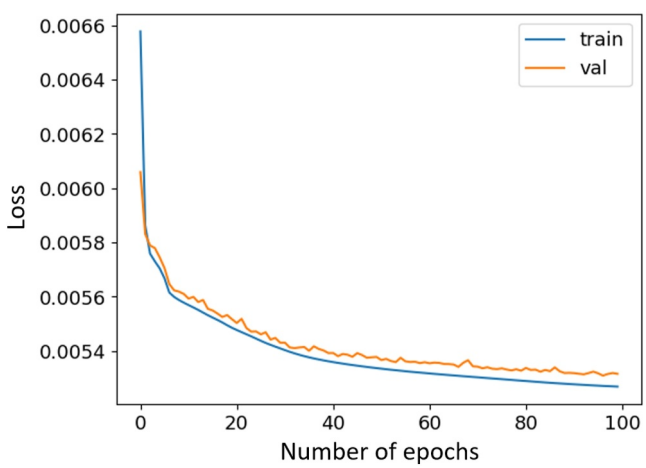

Figure 4. The training and validation loss of the 72 hr input model with no additional parameters, only the historic total electron content (TEC), longitude, latitude, universal time (UT) and day of year (DOY) were used.

3. Methods

3.1. LSTM Architecture

The LSTM is a kind of Recurrent Neural Network (RNN) but has overcome issues like the exploding/vanishing gradient problem by using an appropriate gradient based learning algorithm (Hochreiter & Schmidhuber, 1997). The network can be implemented in Python using Tensorflow (Abadi et al., 2015) and Keras (Chollet et al., 2015) libraries. To overcome the gradient problem, the LSTM uses a forget, input and output gate which is schematically shown in Figure 3. The forget gate contains a sigmoid function to determine how much of the cell state $C_{(t-1)}$ should be remembered by using the output of the sigmoid, which is a value between 0 and 1 and multiply it to the cell state. If the output of the sigmoid is 1, all the information is completely remembered and when the output is 0, it completely forgets. The input gate is determining how much of the input, multiplication of the output of tanh which is a value between −1 and 1 and the sigmoid which gives back a value between 0 and 1, should be remembered by adding it to the cell state. Lastly there is the output gate which controls the output h_t by multiplying the cell state with the current memory information using the same method as the input gate. The cell state C_t and output of the cell h_t, can be described by the following formulas:

10.1029/2024JH000123

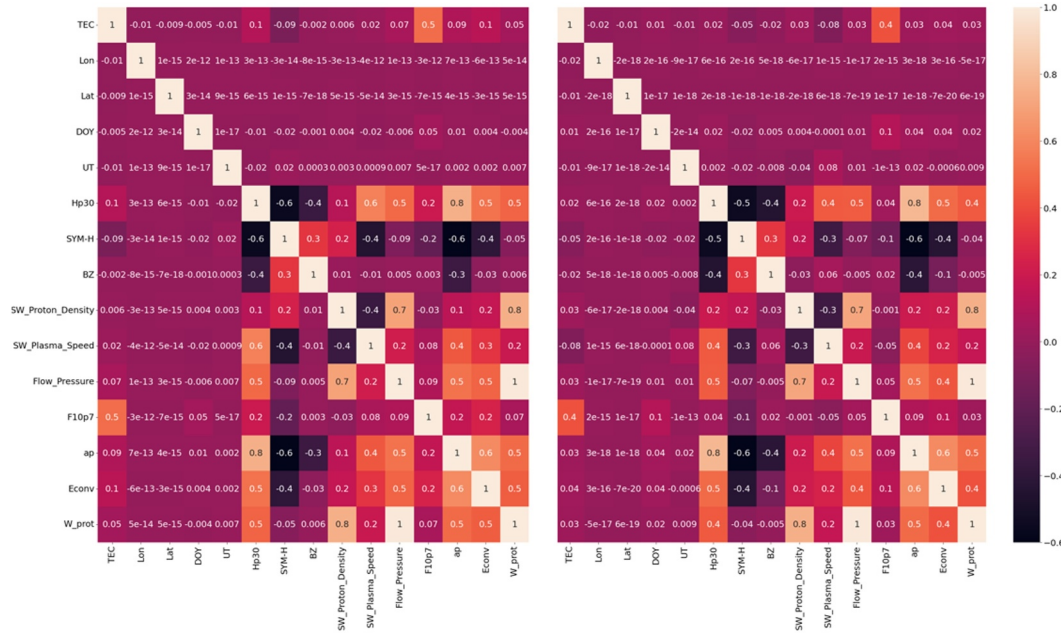

Figure 5. The Pearson's correlation matrix for all data from the last solar cycle (left) and during storm days (right).

$$C_t = C_{t-1} * \sigma\big(W_f(h_{t-1}, x_t) + b_f\big) + \sigma(W_i(h_{t-1}, x_t) + b_i) * \tanh(W_C(h_{t-1}, x_t) + b_C) \tag{4}$$

$$h_t = \sigma(W_o(h_{t-1}, x_t) + b_o) * \tanh(C_t) \tag{5}$$

Where W_f, b_f, W_i, b_i, W_o, b_o, W_C and b_C stand for the weights and biases of the forget, input, output gate and candidate values, respectively.

3.2. Hyperparameter Tuning and Feature Selection

For hyperparameter tuning and feature selection, data from the last solar cycle (2009–2020) was used. In order to find the optimal set of hyperparameters the random grid search method was used, where different settings of the network are randomly set and compared. The hyperparameters that were investigated are shown in Table 1. The selected hyperparameters are shown in bold. The "Adam" optimization function (Kingma & Ba, 2014) is used and

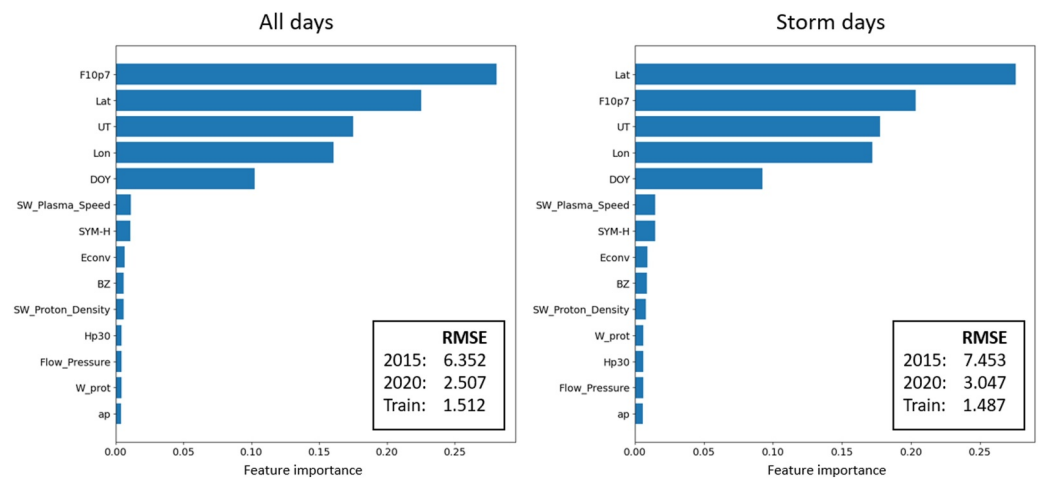

Figure 6. The feature importance from the random forest algorithm for all data (left plot) and storm days (right plot). The root mean square error (RMSE) values are displayed in the right corner of the plots.

Table 2
The Performance of the Proposed Models Trained on Data From the Last Solar Cycle

Model	Input Hours	2015 1	6	12	24	Average
Base	24	1.9 (2.1)	3.6 (4.5)	3.9 (4.9)	3.9 (4.9)	3.7 (4.6)
Base + E_{conv}	24	1.9 (2.1)	3.5 (4.3)	3.8 (4.7)	3.9 (4.7)	3.6 (4.4)
Base + E_{conv} + W_{prot}	24	1.9 (2.1)	3.5 (4.3)	3.7 (4.6)	3.9 (4.6)	3.6 (4.3)
Base	72	1.8 (2.0)	3.5 (4.3)	3.8 (4.6)	3.9 (4.7)	3.4 (4.3)
Base + E_{conv}	72	1.8 (2.0)	3.5 (4.1)	3.7 (4.4)	3.8 (4.5)	3.3 (4.1)
Base + E_{conv} + W_{prot}	72	1.8 (2.1)	3.5 (4.2)	3.7 (4.5)	3.8 (4.5)	3.3 (4.2)
Base + *SYM-H* + *Hp*30 + *F*10.7	72	1.8 (2.0)	3.3 (4.0)	3.6 (4.3)	3.7 (4.5)	3.2 (4.1)

Note. The RMSE values are computed for the test data set which comprises data from the high solar activity year 2015. The value between the brackets is the RMSE during storm periods in the same year and the RMSE is given in TECU.

the loss function is the mean absolute error (MAE). The use of the ReLU activation function did not improve the results, therefore the default setting has been chosen which is the hyperbolic tangent (tanh). There was no sign of overfitting, shown in Figure 4, therefore no regularization term or dropout was added.

To find the optimal set of input parameters, different feature selection techniques have been applied, that is, training different models and comparing the training and validation loss and accuracy, random trees and Pearson's correlation. The Pearson's correlation matrix indicates the linear relationship between the different parameters, shown in Figure 5. Since the model should perform well during storm- and quiet-time periods, a comparison between the whole data set (left plot from Figure 5) and perturbed conditions (right plot from Figure 5) has been made. From the correlation matrix a clear correlation (of 0.5) is seen between the solar flux index *F*10.7 and TEC. There is also some correlation with E_{conv}, *Hp*30 and *SYM-H*. The other parameters do not show a very high correlation. In the right plot of Figure 5 the Pearson's correlation is plotted separately for storm conditions, here only a moderate correlation (of 0.4) with *F*10.7 is seen.

Using the random forest algorithm has the advantage of showing the feature importance and is a more automated way compared to training multiple models and look at the loss and accuracy. The feature importance is computed based on the Gini importance where the higher the value the more important the feature is. Authors in Zewdie et al. (2021) also used the algorithm to find the top five of important parameters and included them into their LSTM network. To implement the random forest algorithm, the Scikit-Learn Python package is used (Pedregosa et al., 2011). The maximum depth of the trees was set to 30. The accuracy of random forest regressors using less tree depth was worse, but using a higher maximum depth would increase the training time significantly. To further speed up the fitting process only 5% of the data from the last solar cycle (2010–2020) was randomly sampled and

Table 3
The Performance of the Proposed Models Trained on Data From the Last Solar Cycle

Model	Input Hours	2020 1	6	12	24	Average
Base	24	1.0 (1.1)	1.8 (2.1)	1.9 (2.1)	1.8 (1.9)	1.8 (2.0)
Base + E_{conv}	24	1.0 (1.0)	1.7 (1.9)	1.8 (2.0)	1.8 (1.8)	1.7 (1.9)
Base + E_{conv} + W_{prot}	24	1.0 (1.0)	1.7 (1.9)	1.8 (2.0)	1.8 (1.8)	1.7 (1.9)
Base	72	0.9 (0.9)	1.6 (1.7)	1.7 (1.7)	1.7 (1.6)	1.5 (1.6)
Base + E_{conv}	72	0.9 (0.9)	1.6 (1.6)	1.6 (1.7)	1.7 (1.6)	1.5 (1.6)
Base + E_{conv} + W_{prot}	72	0.9 (0.9)	1.6 (1.7)	1.6 (1.7)	1.7 (1.6)	1.5 (1.6)
Base + *SYM-H* + *Hp*30 + *F*10.7	72	0.9 (0.9)	1.6 (1.6)	1.6 (1.6)	1.6 (1.6)	1.5 (1.5)

Note. The RMSE values are computed for the test data set which comprises data from the low solar activity year 2020. The value between the brackets is the RMSE during storm periods in the same year and the RMSE is given in TECU.

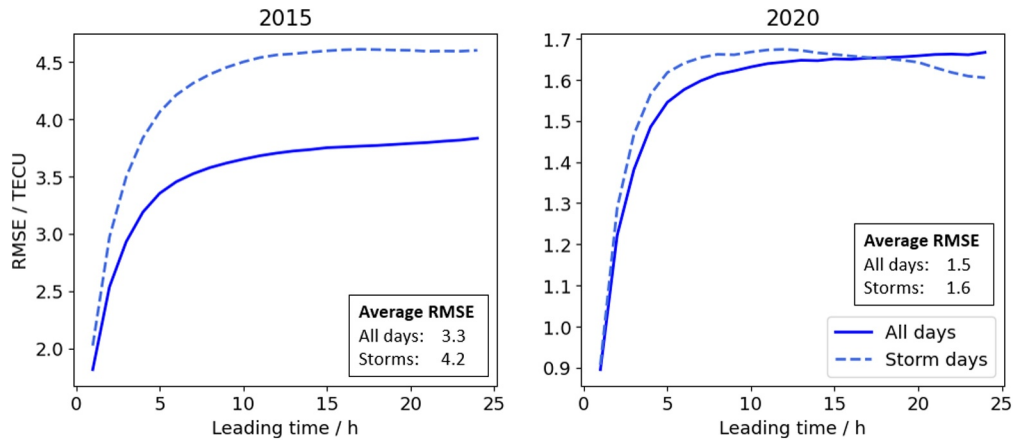

Figure 7. The LSTM-based model RMSE values plotted against the leading time for all days and storm days in 2015 and 2020, respectively.

used for training and testing. We trained two models: one with data for the complete period and another model containing data only during geomagnetic storm periods. The models are tested with independent data sets from 2015 and 2020 which are purposefully excluded from the training data set. The years 2015 and 2020 were chosen due to their different solar activities, for example, 2015 is a year where high solar activity is seen and 2020 a low solar activity year, respectively. The feature importance and the performance of the models (shown in the right corner of the plots) are displayed in Figure 6. We found that the geographic latitude, longitude, solar flux index, universal time (UT) and day of year (DOY) are the most important features in order to predict the TEC. The Pearson's correlation matrix also showed a higher coefficient in case of the solar flux index. However, the latitude is showing the highest importance for the storm days.

In order to compare the model's performance, a number of base models with common input features such as the longitude, latitude, UT and DOY were implemented. However, different combinations of historic TEC (past 1 day or 3 days) data and external drivers were used as follows:

1. Base model with 1-day historic TEC and no external drivers
2. Base model with 1-day historic TEC and E_{conv} and W_{prot} as additional drivers
3. Base model with 1-day historic TEC and E_{conv} as additional driver
4. Base model with 3-day historic TEC and no external drivers
5. Base model with 3-day historic TEC and additionally E_{conv} and W_{prot} as drivers
6. Base model with 3-day historic TEC and additionally E_{conv} as driver
7. Base model with 3-day historic TEC and additionally $F10.7$, $SYM\text{-}H$ and $Hp30$ as drivers

It is worthy to mention that the solar wind forcing parameters E_{conv} and W_{prot} can also be measured at L1 Lagrange point and have the potential of predicting solar impact up to a few hours ahead. The main objective of the present work is to find a model which gives a good performance not only during quiet ionospheric conditions but also perturbed conditions. Therefore, the above models were tested using whole test data sets as well as a separate storm data set from 2015 and 2020. The storm data set was created in our previous work in Adolfs et al. (2022) and it contained almost 400 storms (storm event with $Dst < -50$ nT are only considered) during the period 1998–2020. The storm data set used for testing consists of a total of 33 storms that occurred during 2015 (27 storms) and 2020 (6 storms). The performance of the above mentioned trained models is analyzed in terms of model residuals when comparing model values with the reference data from the UQRG GIMs. Tables 2 and 3 show that the models using 3-day historic TEC data perform slightly better than those with 1-day historic TEC data in terms of RMSE (root mean squared error) during high and low solar activity years 2015 and 2020, respectively. No significant improvement is found when using additional external driver parameters. We found that the base model with 3-day historic TEC data performs very similar to the models using external drivers. Considering this, the base model using 3-day historic TEC data is selected as an operational model for space weather monitoring for further investigation. It is worthy to mention that this paper focuses on modeling using the LSTM architecture, but the FNN architecture was also considered. Therefore, the performance of an FNN-based

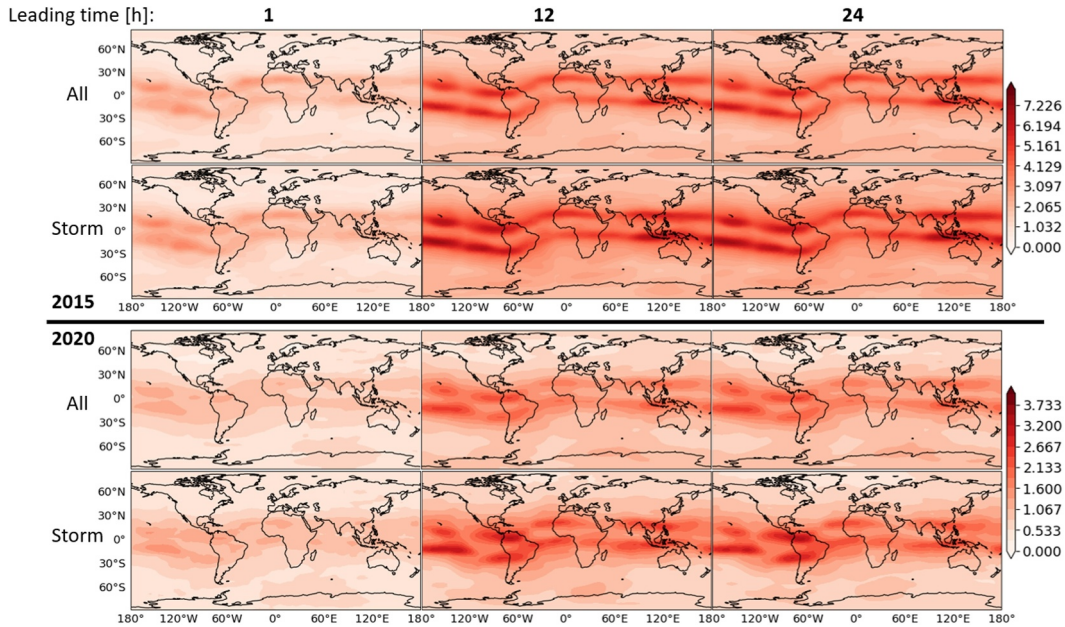

Figure 8. The global RMSE for the complete years (2015 and 2020) and during storm days.

model trained with the same input was compared to the network using the LSTM architecture. The LSTM-based model was outperforming the FNN-based by approximately 0.2 TECU. Therefore, further modeling was continued concentrating only on the LSTM architecture.

The selected model (with 3-day historic TEC data and no external drivers) is trained with data from training cycle one which comprises of data during 1998–2008 and then trained again with the data from training cycle two (2009–2019, 2015 excluded). To avoid overfitting and reduce the training time, the early stopping method was used during training of the final model. Early stopping means that the training procedure is stopped when the validation loss has not gone down for a number of epochs. We used 100 epochs as the maximum number of epochs and training is stopped if the validation loss is not decreasing within 10 epochs. The final model was trained including the validation data set as well with 64 epochs during the first training cycle one and 62 during training cycle two.

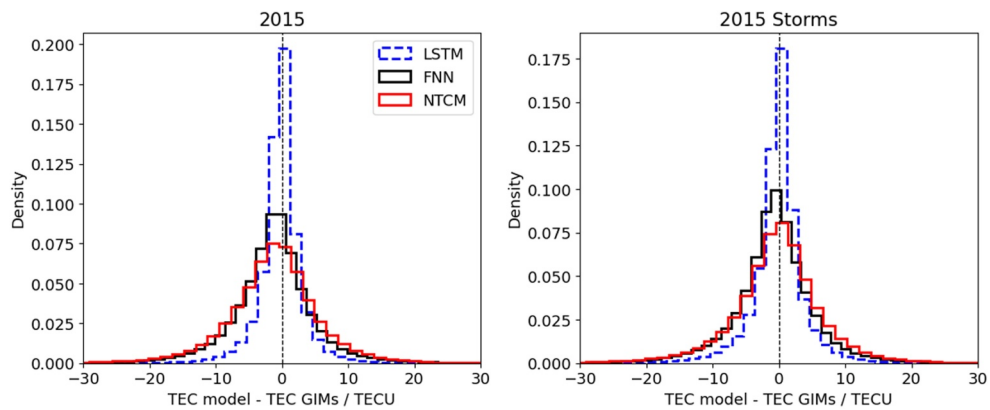

Figure 9. The histograms of the residual errors in 2015. The left plot shows the residual errors for all days in 2015 and the right plot during storm days in 2015 for the LSTM, quiet-time Feed forward neural network (FNN) and Neustrelitz TEC model (NTCM) predictions.

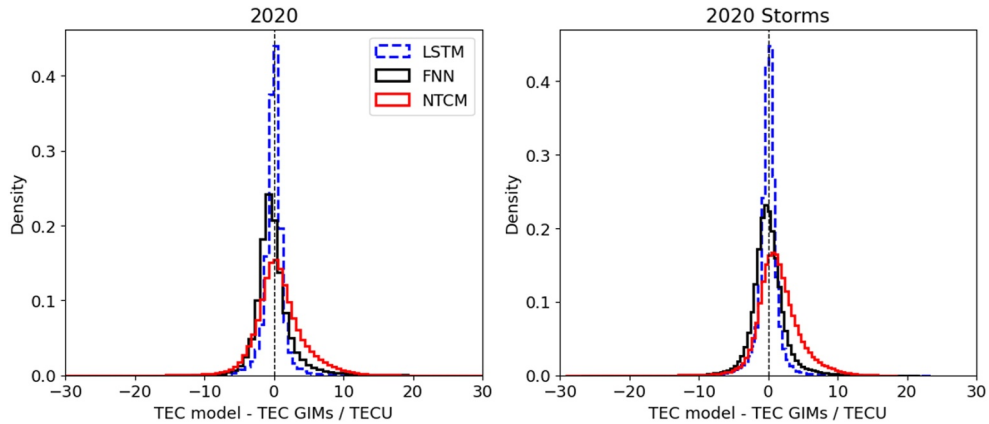

Figure 10. The histograms of the residual errors in 2020. The left plot shows the residual errors for all days in 2020 and the right plot during storm days in 2020 for the LSTM, quiet-time FNN and NTCM predictions.

4. Results

In this section the results of the final model are shown which is driven by the 3-day historic TEC, longitude, latitude, DOY and UT. The performance of the final LSTM-based model is also compared to the FNN-based quiet-time model proposed in Adolfs and Hoque (2021) and the NTCM. The NTCM is a computationally very fast 12 coefficient model, driven by the $F10.7$ index and describes the TEC dependencies on local time, geographic/geomagnetic location, and solar irradiance and activity. The diurnal, semi-diurnal, and ter-diurnal harmonic components are describing the local time dependency. The two crests of increased ionization located at both sides of the magnetic equator (equatorial anomalies) were modeled by Gaussian functions. The proposed LSTM-based model should also be compared to another NN-based model and therefore we used the FNN-based quiet-time model. This model is trained with hourly Carrington rotation averaged (approximately 27 days) data from two solar cycles and is driven by the geographic longitude, geomagnetic latitude, UT, DOY, solar zenith angle and the $F10.7$ index. This model was capable of reproducing the evolution of the small-scale nighttime winter anomaly.

In Figure 7, the variation of the RMSE as a function of forecasting time is plotted for both testing years (2015 and 2020). From this plot we can see that the model's performance is the best when the forecasting time is short. With increasing forecasting time, the model's performance starts rapidly decreasing (i.e., RMSE increasing) until 5 hr leading time. Then, the RMSE slowly increases and reaches up to about 3.8 TECU in case of 2015 and 1.7 TECU in case of 2020 at 24 hr leading time. The average RMSE is found about 3.3 TECU and 1.5 TECU for (considering all days) 2015 and 2020, respectively. During storm days the model is showing higher RMSE values in 2015 (average of 4.2 TECU). During 2020, the model shows a similar performance (RMSE of 1.6 TECU) when considering only storm days and all days (RMSE of 1.5 TECU). The RMSE is even dropping after 15 hr forecasting time in case of the 2020 storm days which can be caused by the fading storm related perturbations as the ionosphere returns to its quiet-time state. However, more investigation is required to know the exact reason of this. The variation in performance between quiet and storm conditions (in 2015) can partially be explained when we compare the storms parameters, for example, *Kp*, $F10.7$ or *Dst*. Stronger negative values for *Dst* are seen during storms that occurred in 2015, together with higher *Kp* and $F10.7$ values. The main difference between the storms occurring in 2015 and 2020, is the solar activity. The year 2015 is a high solar activity period and 2020 is a low solar activity year. The higher ionization levels together with a higher number of storms during the high solar activity period can explain the difference in performance.

Table 4
The Mean and Standard Deviation of the Differences for the LSTM-Based Model, Quiet-Time Feed Forward Neural Network (FNN)-Based Model and Neustrelitz TEC Model (NTCM) for all Days and Storm Days Shown in Brackets

Model	Mean 2015	Std 2015	Mean 2020	Std 2020
LSTM-based model	−0.2 (−0.1)	3.5 (4.3)	−0.1 (0.0)	1.6 (1.6)
FNN-based model	−1.3 (−0.8)	6.1 (6.6)	−0.1 (0.0)	2.7 (2.4)
NTCM	−1.4 (−0.4)	7.4 (7.7)	0.8 (1.5)	3.6 (3.1)

A similar behavior is seen in Figure 8, where the RMSE values are not showing a large difference between 12 hr leading time and 24 hr of leading time. The highest RMSE values are seen around the magnetic equator, where the equatorial anomalies exist which is also seen in Chen et al. (2022). In Figures 9 and 10, the histograms of the TEC differences (i.e., TEC_{model}—

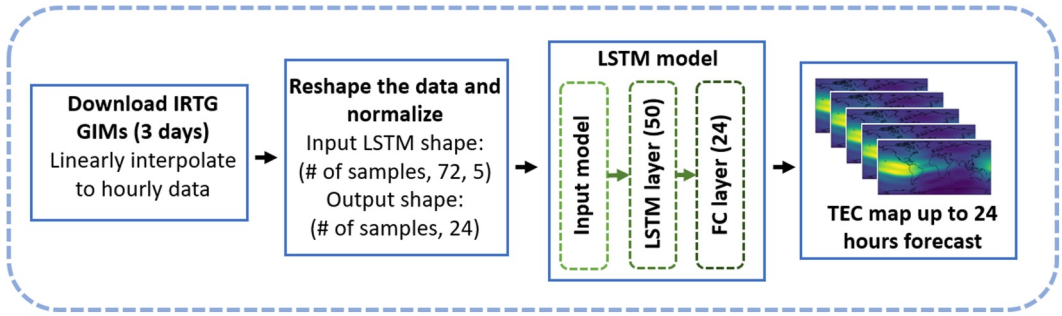

Figure 11. Overview of near real-time application of the LSTM model. Here the LSTM layers are described where the number of neurons, in case of the LSTM and fully connected (FC) layer, are shown between the brackets.

TEC_{ref}) are plotted for the three models. The TEC differences of the LSTM-based model are computed for all predicted TEC values one up to 24 hr ahead, respectively. In Table 4 the mean and standard deviations of the residuals are shown. The models are showing the worst performance during storm time in 2015. The difference between the quiet and storm conditions is not found significant during the low solar activity year 2020. The LSTM-based model is always outperforming the FNN-based model and NTCM.

4.1. Use of LSTM-Based TEC Model for Space Weather Monitoring

In the previous section, UQRG GIMs have been used for training and validation of the network. These maps are available with a 1-day latency. For simulating near real-time (RT) scenarios, GIMs with a smaller latency need to be used. Therefore, the 3-day historic input TEC data are obtained from http://chapman.upc.es/irtg/archive/2022/ (accessed 11 September 2023) which contain the IGS combined RT GIMs product, that is, IRTG. Authors in Liu et al. (2021) found that the RT IRTG GIMs had a similar performance as the IGS rapid solutions (with 1 day latency) and they could be a reliable source for global RT VTEC information. In Figure 11, the workflow used for near real-time application of the LSTM model is shown.

The model output is validated against the final combined solution from IGS (IGSG). These maps are independent and the LSTM-based model has never seen the data before. The model is tested for two storm days (DOY 104 and 105, 2022), two quiet days (DOY 154 and 155, 2022) and two quiet days 1 day after an M-class solar flare (DOY 242 and 243, 2022). The maximum *Kp* and minimum *Dst* values for these days are shown in Table 5. The performance, in terms of RMSE, mean and standard deviation of the differences (TEC_{model}—TEC_{ref}), of the LSTM-based model is compared to the quiet-time model and the NTCM. Both models use the solar flux index in order to make predictions. The solar flux index is provided from the day before for the NTCM and FNN-based model, in order to have fairer RT comparisons. The model performance is shown in Table 5 and in Figure 12. From the table and figure we can see that the LSTM-based model is always outperforming the other two models but the three models generally show a very similar pattern. The NTCM and quiet-time NN model show in almost all cases a larger bias, seen in Figure 12. The quiet-time model is trained with Carrington rotation averaged (approximately 27 days) CODE GIMs which can cause this bias (here IGS combined maps are used as reference). Since both models are driven by the solar flux index, it is expected that they give a higher TEC output when the solar flux index increases, therefore the two models are sensitive to peaks in the solar flux index. In case of the quiet days after a solar flare, the solar flux index has higher values. Therefore, the FNN-based and NTCM models are overpredicting whereas the LSTM-based model gives stable predictions. The performance of the LSTM- and FNN-based model during the quiet days is very similar.

Table 5
The RMSE in TEC Units (TECU) for the LSTM-Based, the Quiet-Time FNN-Based Model and the NTCM

DOY	LSTM	FNN	NTCM	*Kp*(max)	*Dst*(min)
104 (Storm)	5.2	6.4	7.7	6	−81
105 (Storm)	4.7	4.9	6.2	5	−70
154 (Quiet)	2.2	2.6	4.9	1.3	−8
155 (Quiet)	2.4	2.6	5.0	1	−1
242 (Quiet after solar flare)	2.8	7.3	8.5	4	−13
243 (Quiet after solar flare)	2.4	5.8	7.9	4.3	−11

Note. The last two columns show the maximum *Kp* and minimum *Dst* for the corresponding days. *Dst* is given in nano tesla.

5. Summary and Conclusion

In this work a neural network (NN)-based global total electron content (TEC) model is proposed that makes predictions up to 24 hr ahead taking advantage of the long short-term memory (LSTM) architecture. The network was

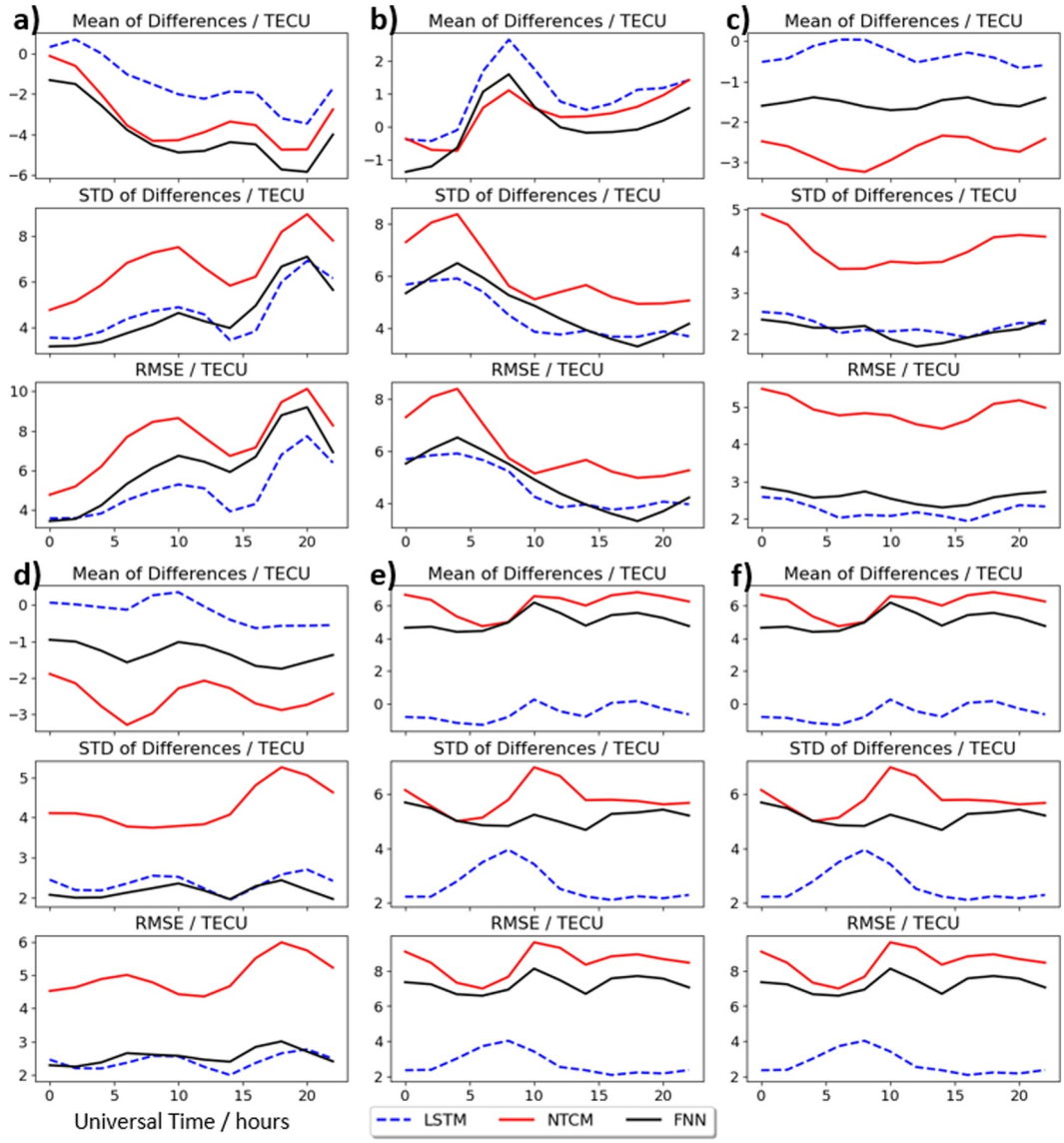

Figure 12. The performance in term of mean, standard deviation and RMSE of the differences for the LSTM-based, quiet-time FNN-based and NTCM model for 14th of April (a), 15th of April (b), 3rd of June (c), 4th of June (d), 30th of August (e) and 31st of August (f) in 2022.

trained, validated and tested with TEC data covering the last two solar cycles obtained from the rapid UQRG global ionosphere maps (GIMs). In this paper, several additional drivers (*SYM-H*, geomagnetic activity index *Hp*30, solar radio flux index *F*10.7, W_{prot} and E_{conv}) were included in order to see whether this would increase the performance of the model significantly or not. The final model uses the historic TEC data (past 3 days), the universal time, longitude, latitude and day of year as model inputs and no additional drivers. The performance of the model was tested for quiet and geomagnetic storm conditions using data from a high solar activity year (HSA) 2015 and low solar activity (LSA) year 2020. The average RMSE is found about 3.3 TECU and 1.5 TECU for (considering all days) 2015 and 2020, respectively. During storm days the model is showing higher RMSE values in 2015 (average of 4.2 TECU). The model's performance for the test data with LSA conditions (2020) stayed almost the same for all data and data during storm conditions with RMSE of about 1.6 TECU. The accuracy of the LSTM-based model was also compared to the quiet-time feed forward NN (FNN)-based model and the Neustrelitz TEC model (NTCM). The results indicate that the LSTM-based model is outperforming both models. Furthermore, the performance of the LSTM-based TEC model was also tested for near real-time (RT) cases by

using International GNSS Service (IGS) RT products as historical TEC inputs and the model performs well during both quiet and perturbed periods and outperforms the FNN-based model and NTCM.

Data Availability Statement

The global ionosphere maps (GIMs) from Universitat Politècnica de Catalunya (UPC) can be downloaded from the Crustal Dynamics Data Information System (CDDIS) (Noll, 2010), available at https://cddis.nasa.gov/archive/gnss/ionex/. The combined final maps (IGSG) were downloaded from CDDIS as well. For downloading from CDDIS with the https protocol, an Earthdata login account is needed. The real-time IRTG GIMs (Liu & Hernández-Pajares, 2022) were obtained from http://chapman.upc.es/irtg/archive/2022/. The *Hp*30 data is downloaded from the GeoForschungsZentrum (Matzka et al., 2022), available at https://www.gfz-potsdam.de/en/hpo-index/. The *SYM-H* data from the World Data Center for Geomagnetism, Kyoto (World Data Center for Geomagnetism et al., 2022) is available at http://wdc.kugi.kyoto-u.ac.jp/aeasy/index.html. The solar flux index *F*10.7, the interplanetary magnetic field components *Bx*, *By*, and *Bz*, the solar wind bulk flow speed v_{sw}, the bulk flow latitude and longitude Lat_{sw}, Lon_{sw} and the proton density ρ_{prot} were downloaded from the OMNIWeb interface (Papitashvili & King, 2020), available at https://omniweb.gsfc.nasa.gov/form/dx1.html. We would like to thank these organizations for making their data publicly available.

Acknowledgments
The authors would like to gratefully acknowledge the use of Python, Scikit-learn, TensorFlow and Keras. We also thank and acknowledge the IGS, UPC, GFZ, Kyoto World Data Center for Geomagnetism, and NASA/GSFC's Space Physics Data Facility's OMNIWeb for their freely available data sets. Open Access funding enabled and organized by Projekt DEAL.

References

Abadi, M., Agarwal, A., Barham, P., Brevdo, E., Chen, Z., Citro, C., et al. (2015). Tensorflow: Large-scale machine learning on heterogeneous systems. Retrieved from https://www.tensorflow.org/

Adolfs, M., & Hoque, M. M. (2021). A neural network-based TEC model capable of reproducing nighttime winter anomaly. *Remote Sensing*, *13*(22), 4559. https://doi.org/10.3390/rs13224559

Adolfs, M., Hoque, M. M., & Shprits, Y. Y. (2022). Storm-time relative total electron content modelling using machine learning techniques. *Remote Sensing*, *14*(23), 6155. https://doi.org/10.3390/rs14236155

Borovsky, J. E., & Denton, M. H. (2006). Differences between CME-driven storms and CIR-driven storms. *Journal of Geophysical Research*, *111*(A7). https://doi.org/10.1029/2005JA011447

Chen, Z., Liao, W., Li, H., Wang, J., Deng, X., & Hong, S. (2022). Prediction of global ionospheric TEC based on deep learning. *Space Weather*, *20*(4). https://doi.org/10.1029/2021SW002854

Chen, Z., Zhou, K., Li, H., Wang, J.-s., Ouyang, Z., & Deng, X. (2023). Global TEC map fusion through a hybrid deep learning model: Rfgan. *Space Weather*, *21*(1), e2022SW003341. https://doi.org/10.1029/2022SW003341

Cherrier, N., Castaings, T., & Boulch, A. (2017). Deep sequence-to-sequence neural networks for ionospheric activity map prediction. In *Neural Information Processing: 24th International Conference, ICONIP 2017, Guangzhou, China, November 14–18, 2017, Proceedings, Part V* (Vol. 24, pp. 545–555). https://doi.org/10.1007/978-3-319-70139-4_55

Chimsuwan, P., Supnithi, P., Phakphisut, W., & Min Myint, L. M. (2021). Construction of LSTM model for total electron content (TEC) prediction in Thailand. In *2021 18th International Conference on Electrical Engineering/Electronics, Computer, Telecommunications and Information Technology (ECTI-CON)* (pp. 276–279). IEEE. https://doi.org/10.1109/ECTI-CON51831.2021.9454881

Chollet, F., et al. (2015). Keras. https://keras.io

Davies, K. (1990). Ionospheric radio.

Gonzalez, W. D., Joselyn, J. A., Kamide, Y., Kroehl, H. W., Rostoker, G., Tsurutani, B. T., & Vasyliunas, V. M. (1994). What is a geomagnetic storm? *Journal of Geophysical Research*, *99*(A4), 5771–5792. https://doi.org/10.1029/93JA02867

Hochreiter, S., & Schmidhuber, J. (1997). Long short-term memory. *Neural Computation*, *9*(8), 1735–1780. https://doi.org/10.1162/neco.1997.9.8.1735

Hoque, M. M., & Jakowski, N. (2015). An alternative ionospheric correction model for global navigation satellite systems. *Journal of Geodesy*, *89*(4), 391–406. https://doi.org/10.1007/s00190-014-0783-z

Hoque, M. M., Jakowski, N., & Berdermann, J. (2017). Ionospheric correction using NTCM driven by GPS Klobuchar coefficients for GNSS applications. *GPS Solutions*, *21*(4), 1563–1572. https://doi.org/10.1007/s10291-017-0632-7

Hoque, M. M., Jakowski, N., & Berdermann, J. (2018). Positioning performance of the NTCM model driven by GPS Klobuchar model parameters. *Journal of Space Weather and Space Climate*, *8*, A20. https://doi.org/10.1051/swsc/2018009

Hoque, M. M., Jakowski, N., & Orús-Pérez, R. (2019). Fast ionospheric correction using Galileo AZ coefficients and the NTCM model. *GPS Solutions*, *23*(2), 41. https://doi.org/10.1007/s10291-019-0833-3

Jakowski, N., Hoque, M. M., & Mayer, C. (2011). A new global TEC model for estimating transionospheric radio wave propagation errors. *Journal of Geodesy*, *85*(12), 965–974. https://doi.org/10.1007/s00190-011-0455-1

Kamal, S., Jakowski, N., Hoque, M. M., & Wickert, J. (2020). E layer dominated ionosphere occurrences as a function of geophysical and space weather conditions. *Remote Sensing*, *12*(24), 4109. https://doi.org/10.3390/rs12244109

Kingma, D. P., & Ba, J. (2014). Adam: A method for stochastic optimization. arXiv preprint arXiv:1412.6980.

Klobuchar, J. (1987). Ionospheric time-delay algorithm for single-frequency GPS users. *IEEE Transactions on Aerospace and Electronic Systems, AES*, *23*(3), 325–331. https://doi.org/10.1109/TAES.1987.310829

Li, L., Liu, H., Le, H., Yuan, J., Shan, W., Han, Y., et al. (2023). Spatiotemporal prediction of ionospheric total electron content based on ED-CONVLSTM. *Remote Sensing*, *15*(12), 3064. https://doi.org/10.3390/rs15123064

Lilensten, J. (2007). In *Space weather: Research towards applications in Europe/edited by Jean Lilensten* (Vol. 344). Springer. Retrieved from http://www.springer.com/gb/BLDSS

Lin, X., Wang, H., Zhang, Q., Yao, C., Chen, C., Cheng, L., & Li, Z. (2022). A spatiotemporal network model for global ionospheric TEC forecasting. *Remote Sensing*, *14*(7), 1717. https://doi.org/10.3390/rs14071717

Liu, Q., & Hernández-Pajares, M. (2022). The archive of IGS combined real-time GIM [Dataset]. Retrieved from http://chapman.upc.es/irtg/archive

Liu, Q., Hernández-Pajares, M., Yang, H., Monte-Moreno, E., Roma-Dollase, D., García-Rigo, A., et al. (2021). The cooperative IGS RT-GIMS: A reliable estimation of the global ionospheric electron content distribution in real time. *Earth System Science Data*, *13*(9), 4567–4582. https://doi.org/10.5194/essd-13-4567-2021

Matzka, J., Bronkalla, O., Kervalishvili, G., Rauberg, J., & Yamazaki, Y. (2022). Geomagnetic Hpo index (Version 2.0) [Dataset]. *GFZ Data Services*. https://doi.org/10.5880/Hpo.0002

Natras, R., Soja, B., & Schmidt, M. (2022). Ensemble machine learning of random forest, AdaBoost and XGBoost for vertical total electron content forecasting. *Remote Sensing*, *14*(15), 3547. https://doi.org/10.3390/rs14153547

Nava, B., Coïsson, P., & Radicella, S. M. (2008). A new version of the nequick ionosphere electron density model. *Journal of Atmospheric and Solar-Terrestrial Physics*, *70*(15), 1856–1862. https://doi.org/10.1016/j.jastp.2008.01.015

Noll, C. E. (2010). The crustal dynamics data information system: A resource to support scientific analysis using space geodesy. *Advances in Space Research*, *45*(12), 1421–1440. https://doi.org/10.1016/j.asr.2010.01.018

Orus Perez, R. (2019). Using tensorflow-based neural network to estimate GNSS single frequency ionospheric delay (IONONET). *Advances in Space Research*, *63*(5), 1607–1618. https://doi.org/10.1016/j.asr.2018.11.011

Papitashvili, N. E., & King, J. H. (2020). Omni hourly data set [Dataset]. *NASA Space Physics Data Facility*. https://doi.org/10.48322/1shr-ht18

Pedregosa, F., Varoquaux, G., Gramfort, A., Michel, V., Thirion, B., Grisel, O., et al. (2011). Scikit-learn: Machine learning in python. *Journal of Machine Learning Research*, *12*, 2825–2830.

Sun, W., Xu, L., Huang, X., Zhang, W., Yuan, T., Chen, Z., & Yan, Y. (2017). Forecasting of ionospheric vertical total electron content (TEC) using LSTM networks. In *2017 International Conference on Machine Learning and Cybernetics (ICMLC)* (pp. 340–344). IEEE. https://doi.org/10.1109/ICMLC.2017.8108945

Tang, J., Li, Y., Ding, M., Liu, H., Yang, D., & Wu, X. (2022). An ionospheric TEC forecasting model based on a CNN-LSTM-attention mechanism neural network. *Remote Sensing*, *14*(10), 2433. https://doi.org/10.3390/rs14102433

World Data Center for Geomagnetism, K., Imajo, S., Matsuoka, A., Toh, H., & Iyemori, T. (2022). Mid-latitude geomagnetic indices ASY and SYM (ASY/SYM indices) [Dataset]. https://doi.org/10.14989/267216

Xiong, P., Zhai, D., Long, C., Zhou, H., Zhang, X., & Shen, X. (2021). Long short–term memory neural network for ionospheric total electron content forecasting over China. *Space Weather*, *19*(4). https://doi.org/10.1029/2020SW002706

Zewdie, G. K., Valladares, C., Cohen, M. B., Lary, D. J., Ramani, D., & Tsidu, G. M. (2021). Data–driven forecasting of low–latitude ionospheric total electron content using the random forest and LSTM machine learning methods. *Space Weather*, *19*(6). https://doi.org/10.1029/2020SW002639